Journal of Non-Newtonian Fluid Mechanics 321 (2023) 105108

Contents lists available at ScienceDirect

Journal of Non-Newtonian Fluid Mechanics

journal homepage: www.elsevier.com/locate/jnnfm

Deformation and breakup of a viscoelastic drop in time-dependent extensional flows with finite inertia

Abhilash Reddy Malipeddi, Anik Tarafder, Kausik Sarkar *

Department of Mechanical and Aerospace Engineering, George Washington University, Washington, DC 20052, United States of America

ARTICLE INFO

Keywords:
Drops
Viscoelastic
FENE
Time-periodic
Extension
Computation
Emulsion

ABSTRACT

The dynamics of a viscoelastic drop suspended in a Newtonian matrix are simulated in two time-periodic extensional flows, an *oscillating extensional flow* (OEF) and a *rotating extensional flow* (REF) at finite inertia. The drop deformation is studied by varying the capillary number (*Ca*), Reynolds number (*Re*), Strouhal number (*St*), and Weissenberg number (*Wi*) with the viscosity and the density ratios being restricted to unity. In OEF, the drop shows a periodically changing deformation alternating its extension axes in response to the imposed flow. In REF, the drop assumes a rotating ellipsoidal shape reaching a steady deformation. Despite their different natures, the two flows share an underlying similarity and result in almost an identical maximum drop deformation at the same values of the non-dimensional parameters. Due to the finite inertia, the time-periodic forcing leads to a resonance response, i.e., a peak in the deformation as a function of *St* when the forcing frequency matches the natural frequency of the system. Variation in viscoelasticity (*Wi*) gives rise to a non-monotonic trend in deformation as well as the phase of the drop response. An ordinary differential equation-based one-dimensional model has been used to successfully describe the qualitative trends of drop response in both flows. It further emphasizes the common physics underlying the two flows. We also investigate the effects of viscoelasticity on drop breakup in a potential vortex, which is a special case of rotating extensional flow with $St = 2$. Viscoelasticity inhibits drop breakup raising the critical capillary number for break up, an effect more pronounced at lower inertia. The deformation at the critical capillary number increases with increasing *Wi* at low *Re* with opposite variation at high *Re*.

1. Introduction

The widespread occurrence of suspensions and emulsions in many industrial and natural phenomena such as blood flow, microfluidics, paint, food, and polymer processing make their rheological properties an important consideration for the scientific community. The overall rheology of an emulsion or a suspension is determined by the microstructure—shape, size, orientation, and material properties of the particles as well as their concentration. Single drop dynamics have historically proved seminal in describing the microstructure of an emulsion since the pioneering work of Taylor [1,2], also offering valuable insights into pair [3,4] and multi-particle [5,6] dynamics. The research literature on drop dynamics has been largely focused on viscous systems [7–10]. Numerical simulations of viscoelastic multiphase systems were attempted starting in the late nineties of the last century [11, 12]. Early investigations were mostly in steady flows, specifically plane shear, and quite a few were restricted to two dimensions [13–15]. The flows with inertia were rarely studied. Here, we explore the unsteady dynamics of a viscoelastic drop subjected to time-periodic extensional flows in the presence of inertia.

Viscoelasticity gives rise to several interesting phenomena such as rod-climbing, die swell, and tube-less siphon effects [16]. Unlike their viscous counterparts, there is insufficient intuition about viscoelastic flows with many interesting observations that remain poorly explained. For example, there were contradictory findings as to whether matrix viscoelasticity increases or decreases drop deformation in shear [17–19], which was later explained by numerical simulations [13,20]. The behavior is shown to be non-monotonic [20]: increasing viscoelasticity decreases drop inclination away from the extensional axis retarding deformation, but a further increase of viscoelasticity results in a strong extensional flow at drop tips enhancing deformation. Using a computer-controlled four-roll mill Milliken and Leal [21] studied the deformation and break-up of viscoelastic drops and characterized the differences observed for Newtonian and viscoelastic drops. Hsu and Leal

* Corresponding author at: Department of Mechanical and Aerospace Engineering, George Washington University 800 22nd Street NW, Washington, DC 20052.
E-mail address: sarkar@gwu.edu (K. Sarkar).

https://doi.org/10.1016/j.jnnfm.2023.105108
Received 26 April 2023; Received in revised form 28 June 2023; Accepted 15 August 2023
Available online 16 August 2023

[22] experimentally studied the shape evolution of the drop in steady planar extension and the subsequent relaxation dynamics. Ramaswamy and Leal [11,23] numerically simulated a V/VE (i.e., a viscous drop in a viscoelastic medium) as well as a VE/V case in uniaxial extension using a FENE-CR model of viscoelasticity. They showed that the drop deformation is determined by a balance between the pressure, viscous, and polymeric stresses obtaining enhanced deformation in a V/VE system compared to a V/V case, but a viscoelastic drop could have lower or higher deformation than a viscous drop in a viscous medium. Li and Sundararaj [24] found that viscoelastic (Boger fluid) drop breakup in a Newtonian (Poly-dimethylsiloxane) matrix in simple shear depends on drop size: a flow direction breakup for larger drops and vorticity direction breakup for smaller ones.

Our group has numerically simulated the deformation and breakup of an Oldroyd-B drop in a Newtonian matrix, i.e. a VE/V [25] as well as a V/VE [20] case in steady shear. We found a monotonically decreasing deformation with increasing viscoelasticity in the first case due to a retarding effect of the drop viscoelasticity but a nonmonotonic response (noted above) in the other. The critical capillary number for breakup mimics the deformation trends. The VE/V case, however, showed nonmonotonicity for high viscosity ratios because of again increasing alignment with the flow [26]. Verhulst et al. [27,28] performed both experiments and numerical simulations to conclude that drop deformation decreases with matrix viscoelasticity but is hardly affected by drop viscoelasticity. A recent detailed Lattice Boltzmann method study by Wang et al. [29] of an Oldroyd-B drop in a Newtonian matrix found results similar to ours [25,26].

Locally a general flow is neither pure shear nor extension, and it is time-dependent. For instance, turbulent flows locally offer oscillating flow fields due to circulation and eddies of all possible scales and frequencies making time-periodic flows an important model system for studying drop dynamics [30,31]. The material response in extension can be significantly different from that in simple shear even for purely Newtonian cases. Taylor observed that the critical *Ca* for drop breakup is much higher in a shear flow than in an extensional flow, i.e., drops break up more easily in extension than in shear. Hopper et al. [32] showed that the transient behavior of viscous and viscoelastic drops in uniaxial extensional flow is noticeably different. We have previously investigated the dynamics of drops in periodic extensional flows for purely Newtonian cases [31,33–35], uncovering atypical behaviors such as a negative normal stress elasticity in extension [34] at finite inertia.

As a model system, we chose here to focus on time-periodic extensional flows for their influence on a viscoelastic drop. In contrast to the steady case, the axis of extension rotates resulting in a competition between flow-induced stretching and interfacial tension [31]. Two different flows–oscillating extensional flow (OEF) and rotating extensional flow (REF)–are considered [30,31,33–35]. An OEF can be generated experimentally in a four-roll mill [36–38]. An REF is harder to generate experimentally, but it is a generalization of the local flow at a material point moving in a potential vortex, which was originally proposed Deiber and Schowalter [39] as a non-viscometric flow for measuring rheological response. Even though the flows are different, OEF and REF have been shown to generate similar responses from drops [30]. Also, note that recent studies [40–42] attempted to infer viscoelastic material properties from the oscillation dynamics of viscoelastic drops. We have previously performed a preliminary two-dimensional simulation of a Maxwell drop in periodic extensional flows [30]. The restriction to two-dimensional computation severely limited its value. Here, it is extended to three dimensions choosing a more realistic FENE (finite extensible nonlinear elastic) model for the viscoelasticity. We also study possible drop breakups not considered in the previous two-dimensional study.

2. Governing equations and numerical method

A three-dimensional front-tracking finite difference method [43,44] is used to solve the multiphase system containing a drop of one viscoelastic liquid suspended in another viscous liquid. We have used this method to study various problems involving viscous [31,33–35,45–49] and viscoelastic [20,25,26,50–54] fluids. The theoretical basis of the model and the details of the numerical implementation have been presented in detail in previous articles [53]. The multiphase flow problem is recast as a single fluid with spatially varying fluid properties. The interface is tracked explicitly using interconnected Lagrangian markers. The flow in the entire domain is governed by the incompressible Navier-Stokes equations:

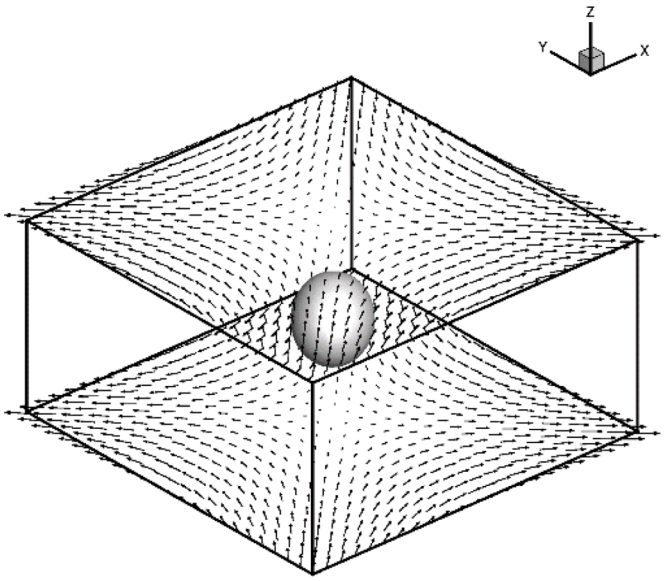

Fig. 1. The computational domain with the drop in the middle, with vectors showing a planar extensional velocity field.

$$\nabla\cdot\mathbf{u} = 0, \tag{1}$$

$$\frac{\partial(\rho\mathbf{u})}{\partial t} + \nabla\cdot(\rho\mathbf{u}\mathbf{u}) = \nabla\cdot\boldsymbol{\tau} - \int_{\partial B}\mathbf{dx_B}\kappa\mathbf{n}\Gamma\delta(\mathbf{x}-\mathbf{x}_B). \tag{2}$$

The (spatially varying) density is denoted by ρ, and the velocity vector field is denoted by $\mathbf{u}$. Γ is the coefficient of interfacial tension, κ is the mean curvature of the interface, and $\mathbf{n}$ is the unit vector locally perpendicular to the drop interface ∂B. $\delta(\mathbf{x})$ is the Dirac delta function. The normal stress jump at the interface is implemented as a singular force term through the integral involving the delta function at the drop interface in the momentum equation [43,55]. The FENE-CR (Finite Extensible Non-linear Elastic-Chilcott and Rallison) [56] equation is used to model the viscoelasticity leading to the total stress comprised of the pressure, polymeric stress, and viscous stress as:

$$\boldsymbol{\tau} = -p\mathbf{I} + \mathbf{T}^p + \mathbf{T}^u,\ \mathbf{T}^u = \mu_s\mathbf{D}, \mathbf{D} = \nabla\mathbf{u} + (\nabla\mathbf{u})^T, \tag{3}$$

$$\frac{\partial\mathbf{A}}{\partial t} + \mathbf{u}\cdot\nabla\mathbf{A} = \nabla\mathbf{u}\cdot\mathbf{A} + \mathbf{A}\cdot(\nabla\mathbf{u})^T - \frac{f}{t_{VE}}(\mathbf{A}-\mathbf{I}), \tag{4}$$

$$\mathbf{T^p} = \left(\frac{\mu_p f}{t_{VE}}\right)(\mathbf{A}-\mathbf{I}), f = \frac{L^2}{L^2 - tr(\mathbf{A})}, \tag{5}$$

Here, the superscript `T' denotes the transpose of a tensor, and $tr(\cdot)$ is the trace operator. μ_s is the solvent viscosity in the non-Newtonian phase and the usual viscosity in the Newtonian phase. The polymeric viscosity of the viscoelastic fluid is denoted by μ_p. The other parameters in the FENE-CR model are the relaxation time (t_{VE}) and the limiting length (L). As in our previous publications we use a modified version of the FENE-CR (FENE-MCR) model, used widely in numerical simulations of viscoelastic flows [57–62]. The simplification executed in the FENE-MCR

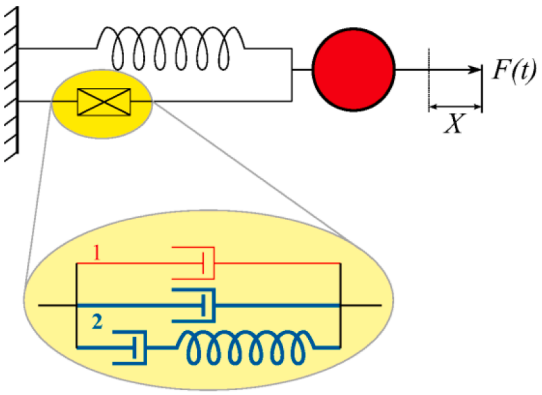

Fig. 2. A sketch of the ODE model for the drop deformation. The viscosity in this model comes from (1) the surrounding fluid and (2) an Oldroyd-B element for the drop.

numerical algorithm and its validity have been described in detail in our previous publications [4,53,54,63]. The governing equations are discretized and solved using a finite difference method.

The drop is suspended at the center of a computational box of size (*10R,10R,5R*) where `*R*' is the drop radius (Fig. 1). The domain is discretized into a uniform $96 \times 96 \times 48$grid. The interface is represented by piecewise linear unstructured triangular elements, separate from the underlying three-dimensional grid. The nominal edge length of the front mesh is kept at ~*0.8* times the length of a grid segment by an adaptive regridding. Detailed studies performed previously have shown that this level of discretization is adequate for an accurate solution for the present conditions [20,25,26,50–53,63].

3. Problem setup

Here we investigated a drop deforming in two time-periodic flows, a rotating extensional flow and an oscillating extensional flow. A rotating extensional flow (REF) is a planar extension with rotating axes of extension [30]:

$$\mathbf{u}_{RE} = \dot{\gamma}\begin{pmatrix} \sin\omega t & -\cos\omega t & 0 \\ -\cos\omega t & -\sin\omega t & 0 \\ 0 & 0 & 0 \end{pmatrix}\begin{pmatrix} x \\ y \\ z \end{pmatrix}. \tag{6}$$

An oscillating extensional flow (OEF), on the other hand, has the axes fixed but the directions of extension and contraction alternate [30]:

$$\mathbf{u}_{OE} = -\dot{\gamma}\cos\omega t\begin{pmatrix} 0 & 1 & 0 \\ 1 & 0 & 0 \\ 0 & 0 & 0 \end{pmatrix}\begin{pmatrix} x \\ y \\ z \end{pmatrix}. \tag{7}$$

There are two notable differences in the flows. First, OEF (as noted before realizable in a four-roll mill) has an instant of zero velocity in each period (whenever $\cos\omega t$ is zero), when the velocity changes sign. REF in contrast has a constant non-zero magnitude of velocity in the entire period. Second, in REF the drop stretches in all directions in the plane as the flow axis rotates, whereas in OEF the drop stretches in the same two directions (the flows can be seen in Figs. 3 and 4 the Results section). We simulate these flows by applying the velocities (6) and (7) at the boundary of the domain as boundary conditions for the velocity in the x and y directions. The z-direction boundary is taken to be periodic. The problem is non-dimensionalized using drop radius, R, as the length scale and inverse of strain-rate, $\dot{\gamma}^{-1}$, as the time scale resulting in the non-dimensional parameters: Reynolds number $\mathrm{Re} = \rho_m \dot{\gamma} R^2 / \mu_m$, Capillary number $Ca = \mu_m \dot{\gamma} R/\sigma$, Weissenberg number, $Wi = t_{VE}\dot{\gamma}$, viscosity ratio $\lambda_\mu = \mu_d/\mu_m$, density ratio $\lambda_\rho = \rho_d/\rho_m$, the ratio of polymeric to total viscosity inside the drop,$\beta = \mu_p/\mu_d = \mu_p/(\mu_p + \mu_s)$ of the drop, and Strouhal number $St = \omega/\dot{\gamma}$. ω is the angular/circular frequency. The subscripts d and m refer to the drop and matrix respectively. μ_s is the solvent viscosity inside the drop. For a drop of alcohol insoluble in water (σ, 1–10 dynes cm^{-1} ([64] p. 17), of radius 100 μm with a shear rate 100 s^{-1}, one obtains $Re = 1$, Ca ~0.01–0.001 and $St = 2$–10. For the results presented here, we have restrictedλ_μ and $\lambda_\rho$fixed at unity, andβ at 0.5.

4. A one-dimensional model for drop response

While the deformation of a drop in a time-periodic velocity field is a complex multiphase flow governed by PDEs (1)–(5), we have previously shown that an ordinary differential equation (ODE) model is useful in understanding the observed dynamics behaviors in the linear limit [30, 65]. Even though the two flows considered here, REF and OEF, are very different, their time-periodic nature underscores an underlying symmetry brought out by the single simplified ODE model for both. In our previous work, we used a model appropriate for an upper-convected Maxwell (UCM) model of drop viscoelasticity. Here, we extend it to a linearized Oldroyd model appropriate for the FENE-MCR model of the viscoelasticity in the simulation (Fig. 2). It is used to explain the simulation results. A drop of radius, $\widehat{R}$, subjected to an extensional flow is considered to be a driven damped spring-mass system with mass $\widehat{\rho}\widehat{R}^3$, damping coefficient $\widehat{\mu}\widehat{R}$, and spring stiffness $\widehat{\sigma}$(coefficient of interfacial tension). The parameters associated with the ODE model are distinguished with the hat (ˆ) symbol. For a forcing flow $G_0 g(t)$,$g(t) = \exp(i\widehat{S}\widehat{t}t)$, the deformation of such a drop is given by

$$\begin{aligned} &\widehat{\rho}\widehat{R}^3\ddot{X} + \widehat{\mu}\widehat{R}\dot{X} + \widehat{\sigma}X = \widehat{\mu}\widehat{R}G_0 g(t) + \widehat{\rho}\widehat{R}^3 G_0 \dot{g}(t), \\ &\text{with} \dot{X}(0) = G_0 g(0), X(0) = 0, \end{aligned} \tag{8}$$

as the initial conditions. Note that X has a dimension of length and is scaled by $\widehat{R}$. The time is scaled by $\widehat{R}/G_0$. The ODE model Eq. (8) is similar to the one in our previous article [66]. The first term represents inertia, the second a viscous response, and the third one is resistance due to interfacial tension. On the left-hand side, the forcing terms are collected, the first one corresponding to the viscous stress$\mu\dot{\gamma}$arising from the imposed flow. The second forcing term arises from the pressure (a time-dependent velocity gives rise to pressure $\rho\partial\mathbf{u}/\partial t \sim \nabla p$). To account for the viscosity and density of both the drop and the surrounding fluid, we assume an equal contribution from the drop and the surrounding fluid to our ODE model, replacing $\widehat{\mu}$ by $(\widehat{\mu}_d + \widehat{\mu}_m)/2$and $\widehat{\rho}$ by $(\widehat{\rho}_d + \widehat{\rho}_m)/2$. Upon non-dimensionalization, it results in

$$\left(\frac{1+\widehat{\lambda}_\rho}{2}\right)\widehat{\mathrm{Re}}\ddot{X} + \left(\frac{1+\widehat{\lambda}_\mu}{2}\right)\dot{X} + \frac{1}{\widehat{Ca}}X = g(t) + \widehat{\mathrm{Re}}\dot{g}(t), \tag{9}$$

where$\widehat{\mathrm{Re}} = \rho_m \widehat{R} G_0/\widehat{\mu}_m$, $\widehat{Ca} = \widehat{\mu}_m G_0/\widehat{\sigma}$. For a viscoelastic drop, the stress is given by Eqs. (4) and (5). Linearization and scaling of the viscoelastic constitutive relation (Eqs. (4) and (5)) to a linearized Oldroyd-B type relation, we get the polymeric contribution to force $(\widehat{T}^p)$ as

$$\widehat{Wi}\frac{\partial \widehat{T}^p}{\partial t} + \widehat{T}^p = \widehat{\mu}_p \widehat{D}, \text{ or } \widehat{T}^p = \frac{\widehat{\mu}_p}{1 + i\widehat{W}i\,\widehat{S}t}\widehat{D}, \tag{10}$$

where a time-periodic solution $\widehat{T}^p \sim e^{(i\widehat{S}tt)}$ is assumed. The total force $(\widehat{T})$ becomes

$$\widehat{T} = \left(\widehat{\mu}_s + \frac{\widehat{\mu}_p}{1 + i\widehat{W}i\,\widehat{S}t}\right)\widehat{D} \text{ or } \widehat{T} = \left(1 - \widehat{\beta} + \frac{\widehat{\beta}}{1 + i\widehat{W}i\,\widehat{S}t}\right)\widehat{\mu}_d\widehat{D} = \widehat{\mu}_{eff}\widehat{D} \tag{11}$$

where $\widehat{\beta} = \widehat{\mu}_p/\widehat{\mu}_d = \widehat{\mu}_p/(\widehat{\mu}_p + \widehat{\mu}_s)$. $\widehat{\beta} = 1$ corresponds to an upper convective Maxwell model (UCM) used in our prior 2D investigation [30] For the ODE model, Eq. (11) can be interpreted to be the constitutive equation for the viscoelastic drop, with an effective complex viscosity $\widehat{\mu}_{eff}$ and substituted in Eq. (9) to obtain the final equation for the model problem. For a time-periodic solution $X = \widetilde{X}e^{(i\widehat{S}tt)}$, one finds

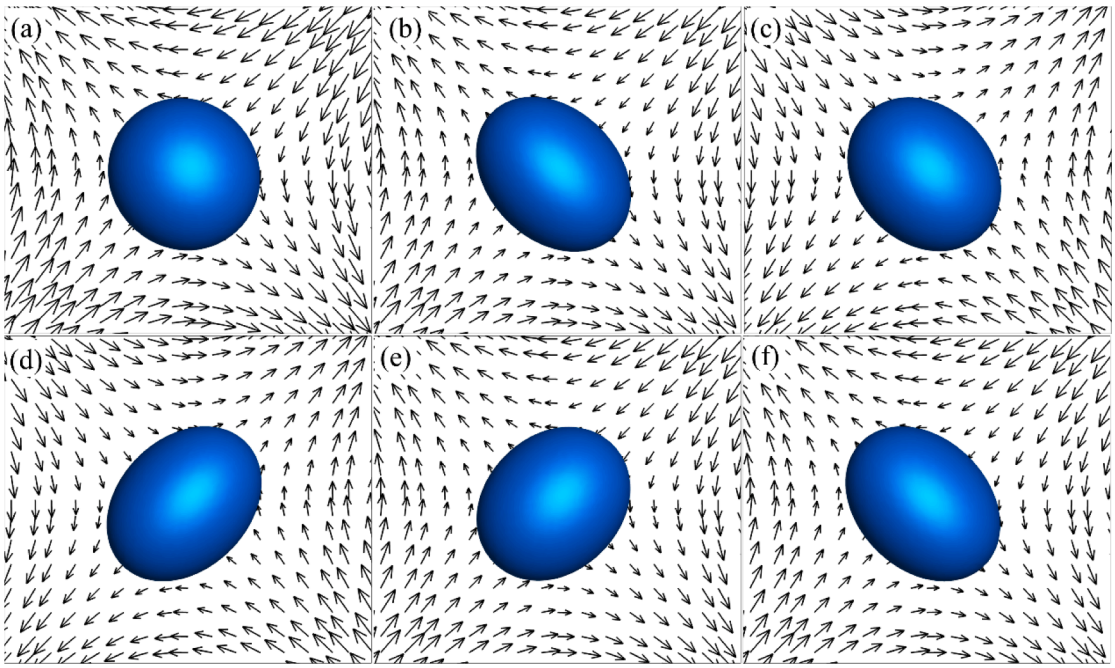

Fig. 3. Drop deformation and velocity field in the central xy-plane for OEF at different instances in one time period for $Re = 1.0$, $St = 2\pi$, $\mathrm{Wi} = 0.2$, and $\mathrm{Ca} = 0.4$.

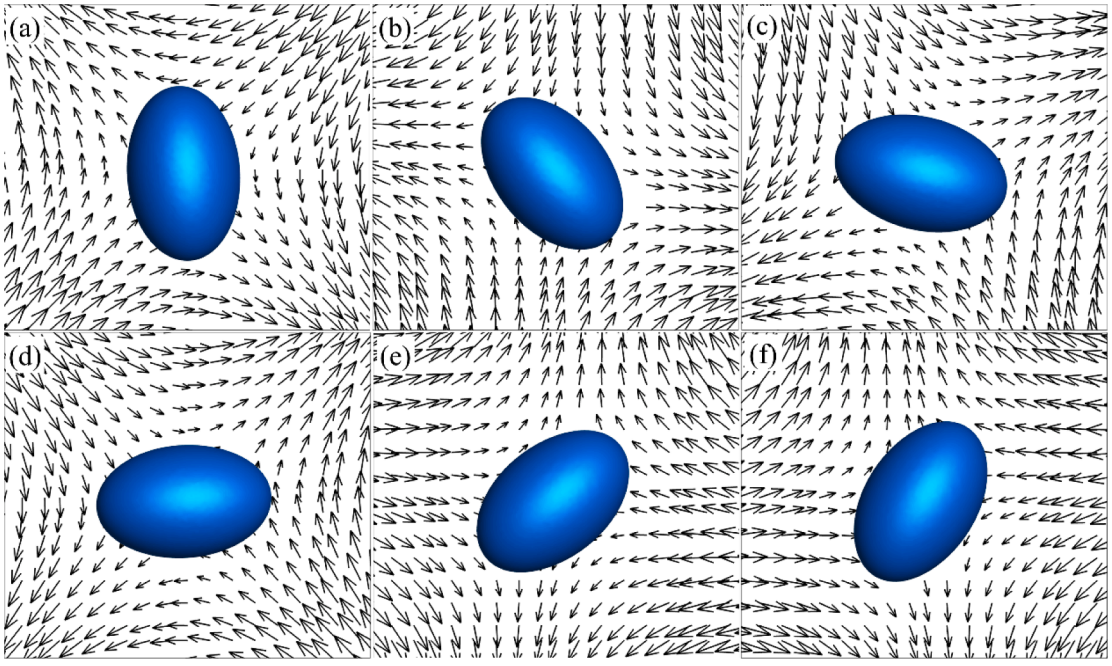

Fig. 4. Drop deformation and velocity field in the central xy-plane for REF at different instances in one time period for $Re = 1.0$,$St = 2\pi$, $\mathrm{Wi} = 0.2$, and $\mathrm{Ca} = 0.4$. Note that the drop is not `tumbling.' The deformation of the drop (the long axis) lags the forcing flow.

$$\widetilde{X} = \frac{1 + \mathrm{i}\widehat{Re}\widehat{St}}{-\frac{1}{2}(1+\lambda_\rho)\widehat{Re}\widehat{St}^2 + \frac{\mathrm{i}}{2}\widehat{St}\left[1 + \lambda_\mu\left(1 - \widehat{\beta} + \frac{\widehat{\beta}}{1+i\widehat{St}\widehat{Wi}}\right)\right] + \widehat{Ca}^{-1}}$$

which for density and viscosity matched system ($\widehat{\lambda}_\mu = \widehat{\lambda}_\rho = 1$) results in

$$\widetilde{X} = \frac{1 + i\widehat{Re}\widehat{St}}{\frac{1}{2}i\widehat{St}\left(2 - \widehat{\beta} + \frac{\widehat{\beta}}{1+i\widehat{St}\widehat{Wi}}\right) - \widehat{Re}\widehat{St}^2 + \widehat{Ca}^{-1}} \tag{12}$$

For a viscous case ($\widehat{\beta} \to 0$) it reduces to

$$\widetilde{X}_{Newtonian} = \frac{1 + i\widehat{Re}\widehat{St}}{i\widehat{St} - \widehat{Re}\widehat{St}^2 + \widehat{Ca}^{-1}} \tag{13}$$

On the other hand, for a Stokes flow ($\widehat{Re} \to 0$) situation, it reduces to

$$\widetilde{X} = \frac{1}{\frac{1}{2}i\widehat{St}\left(2 - \widehat{\beta} + \frac{\widehat{\beta}}{1+i\widehat{St}\widehat{Wi}}\right) + \widehat{Ca}^{-1}}$$

We compute the amplitude and phase of this surrogate response function to understand the simulated dynamics of a drop.

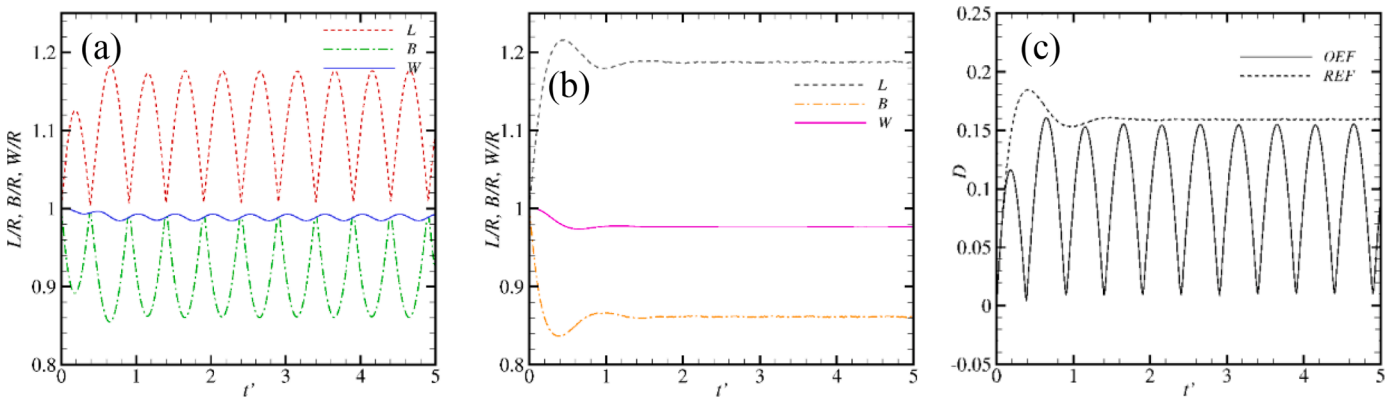

Fig. 5. Evolution of the three axes of the drop with time in OEF (a) and REF (b). (c) Evolution of drop deformation with time in both OEF and REF. All computations are for $Re = 1$, $\mathrm{St} = 2\pi$, $\mathrm{Wi} = 0.2$, $\mathrm{Ca} = 0.4$.

5. Results

5.1. Drop shapes

In the first two sections, we restricted the parameter range to obtain a bounded drop shape. Note that the periodic forcing increases the critical capillary number for breakup compared to the steady extension. Fig. 3 shows the velocity vectors and drop shape at various times within one period (T) after a periodic steady state is reached in an OEF for the case of $Re = 1.0$, $\mathrm{Ca} = 0.4$, $St = 2\pi$, and $Wi = 0.2$ as a typical case. The drop follows the time-periodic extension like the case of a viscous drop [33]. For the same parameter set, Fig 4 shows the corresponding case of a drop in an REF. The deformation of the drop follows the flow with a phase lag—the major axis of the drop trails the extension direction. As is well recorded in a shear flow, the drop obtained an approximately ellipsoidal shape for moderate deformations [67]. The drop shape can be described in terms of the three axes of the ellipsoid—the maximum L and the minimum B distances of the surface of the drop from the centroid, and the half-width W in the z-direction. L and B always lie on the plane of extension for a viscous drop [25]. The drop axes are plotted against time in Fig. 5 (a) and (b). For an OEF, starting from a spherical shape, the drop reaches a periodic steady state, with L (B) reaching a maximum (minimum) twice in each period. There is a small variation in W indicating that the drop is not deforming much in the z-direction, similar to the case of a viscous drop [33]. In contrast, for REF all three axes reach steady values indicating little change in shape but a tumbling shape (Fig. 4).

Fig. 5(c) plots Taylor's deformation parameter [2] $D = (L - B)/(L + B)$ to quantify the drop deformation. Like in Fig. 5(a), D has two maxima in each period in an OEF and a steady value in REF with slight oscillations ($\sim$ 2% of the mean value).

5.2. Drop response

The maximum deformation $D_{\max}$, after a periodic steady state is reached, is plotted against Wi in Fig. 6(a) for $St = 2\pi$, $Ca = 0.125$ and different Re. Although OEF and REF at the outset are different imposed flows—one periodically extending and contracting the drop and the other rotating—there is an underlying similarity [30,65,66]. As a result, the drop response results in similar values of deformation for both flows as a function of Wi—almost identical for the lowest $Re = 0.1$ and differing the most for the highest $Re = 10$. Note the maximum deformation in OEF reaching the steady deformation value in REF in Fig. 5(c). Unlike REF, in OEF the axes of stretching and contraction alternate leading to undulation in deformation and, therefore, a lower response, as we can see in Fig. 6(a). One can anticipate that REF will promote drop breakup for low values of rotation, i.e., smaller St values. The effect of Wi on drop deformation is quite complex and involves a delicate balance between inertia, stretching, rotation, and viscoelastic relaxation time. Depending on which of the terms dominates, the effect of Wi on drop deformation can be completely different as can be seen by different trends for the three Re values. The effect of Wi variation is more prominent at lower inertia (compare $Re = 0.1$, 1.0 against $Re = 10$).

Fig. 6(b) shows the response of the ODE model for the same cases, noting that the same model captures both two periodic flows. The ODE model, due to the severe dimensionality reduction and its linear nature, cannot be expected to offer a quantitative match with the actual results. However, as a proxy for the deformation, it approximately matches the trends with Re and Wi. Specifically, it captures the $Re = 0.1$ quite well. For $Re = 10$ (Fig. 6a), note that the REF and OEF differ the most due to higher deformation for REF and, therefore, the increasing nonlinear effects there are beyond the capabilities of the periodic linearized ODE model which doesn't differentiate between the two. Note that the term due to viscoelasticity (12) contributes to both the real and imaginary parts when compared to a purely Newtonian case. Fig. 6(c) and (d) show the same cases for a higher St ($=4\pi$). Eq. (12) shows that with increasing inertia, i.e., Re increasing, the Wi dependence wanes, as we see also in the simulation results (Fig. 6(a) and (c)).

As an oscillating system at finite inertia, the drop response shows a phase difference with the excitation, as can be assessed from Fig. 3—when the imposed flow momentarily vanishes as it changes from extension to a contraction in one of its axes, the drop deformation is not zero. This is more apparent in Fig. 4, where the long axis of the drop lags the extension direction of the flow. In the case of oscillating extensional flow, this phase difference can be obtained from the deformation parameter D vs. time data. The same method does not work for REF because D may be constant in time. Here, it can be found by calculating the angle between the extension direction of the flow and the orientation of the long axis of the drop.

The phases are plotted in Fig 6(e) for both OEF and REF for different Re values and the two St's. Fig. 6(f) plots the corresponding phase lag predicted by the ODE model, showing a good qualitative agreement with the computational results in Fig. 6(e). In a finite inertia system, there is a sharp change in the phase lag with changing St near the resonance. The ODE model is nevertheless able to capture the variation of phase with Wi. Phase shows a non-monotonic response with Wi. Phase lag is higher at higher Strouhal numbers (Fig. 6e). Increase in Strouhal number increases the inertia term in the ODE model. As a result, at higher Strouhal numbers the phase lag between successive Re (0.1, 1.0, 10) is higher. A close observation of Fig. 6(c) and (e) would reveal that at $St = 4\pi$ drop deformation and phase have a close relationship between them with stronger effects at lower inertia ($Re = 0.1$,1.0) than at the higher value of $Re = 10$. In the range, $Wi = 0.1$–1, where the drop is more in phase with the imposed flow drop, deformation shows higher values.

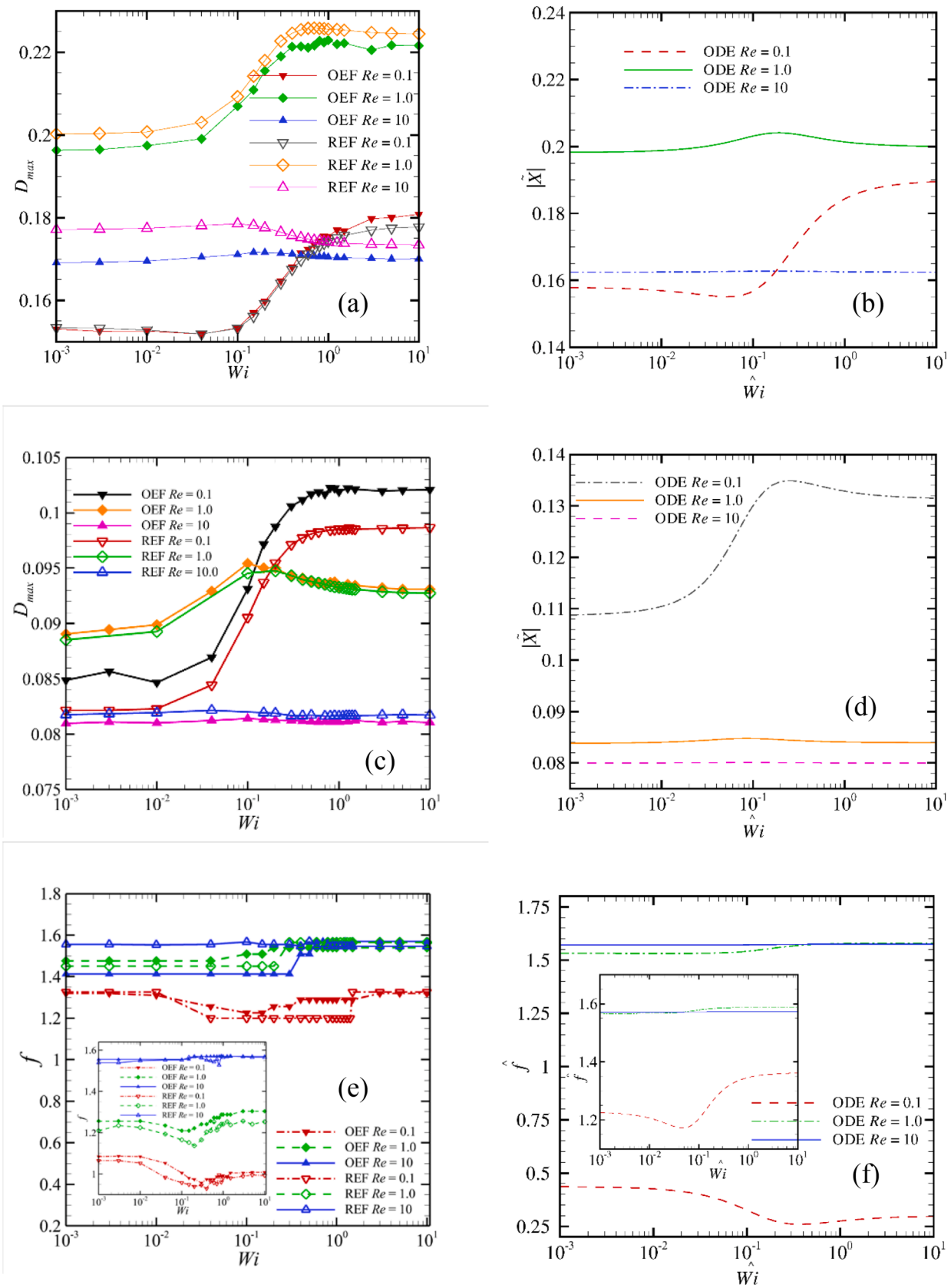

Fig. 6. (a) & (b) Variation of D_{max} (simulation) and $|X|$(ODE model) with Wi for different *Re* at Ca = 0.125, $St = 2\pi$ in OEF and REF. (c) & (d) The same for Ca = 0.125, $St = 4\pi$. (e) & (f) Phase lag between the drop deformation and imposed strain rate vs. Wi for different *Re* at Ca = 0.125, $St = 4\pi$ (Inset shows the same for Ca = 0.125, $St = 2\pi$).

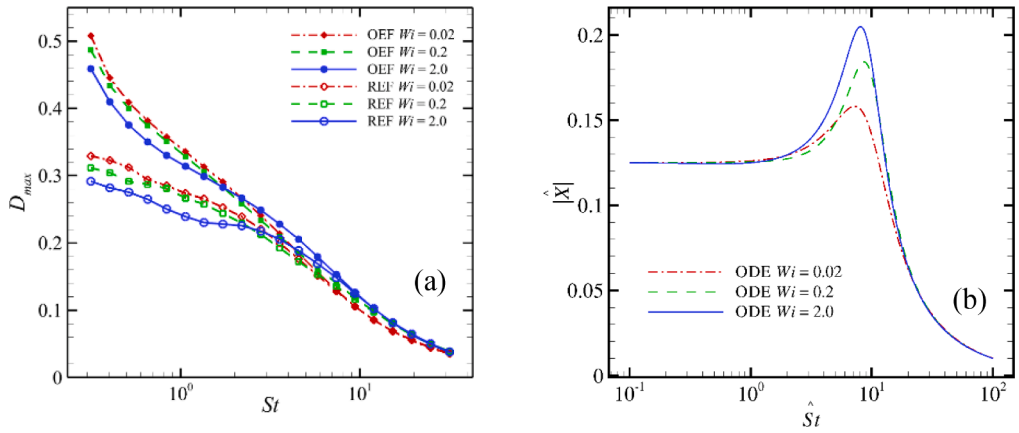

Fig. 7. Deformation vs. St for different Wi for $Re = 0.1$ and $Ca = 0.1$ in OEF and REF from computation (a) and from ODE (b).

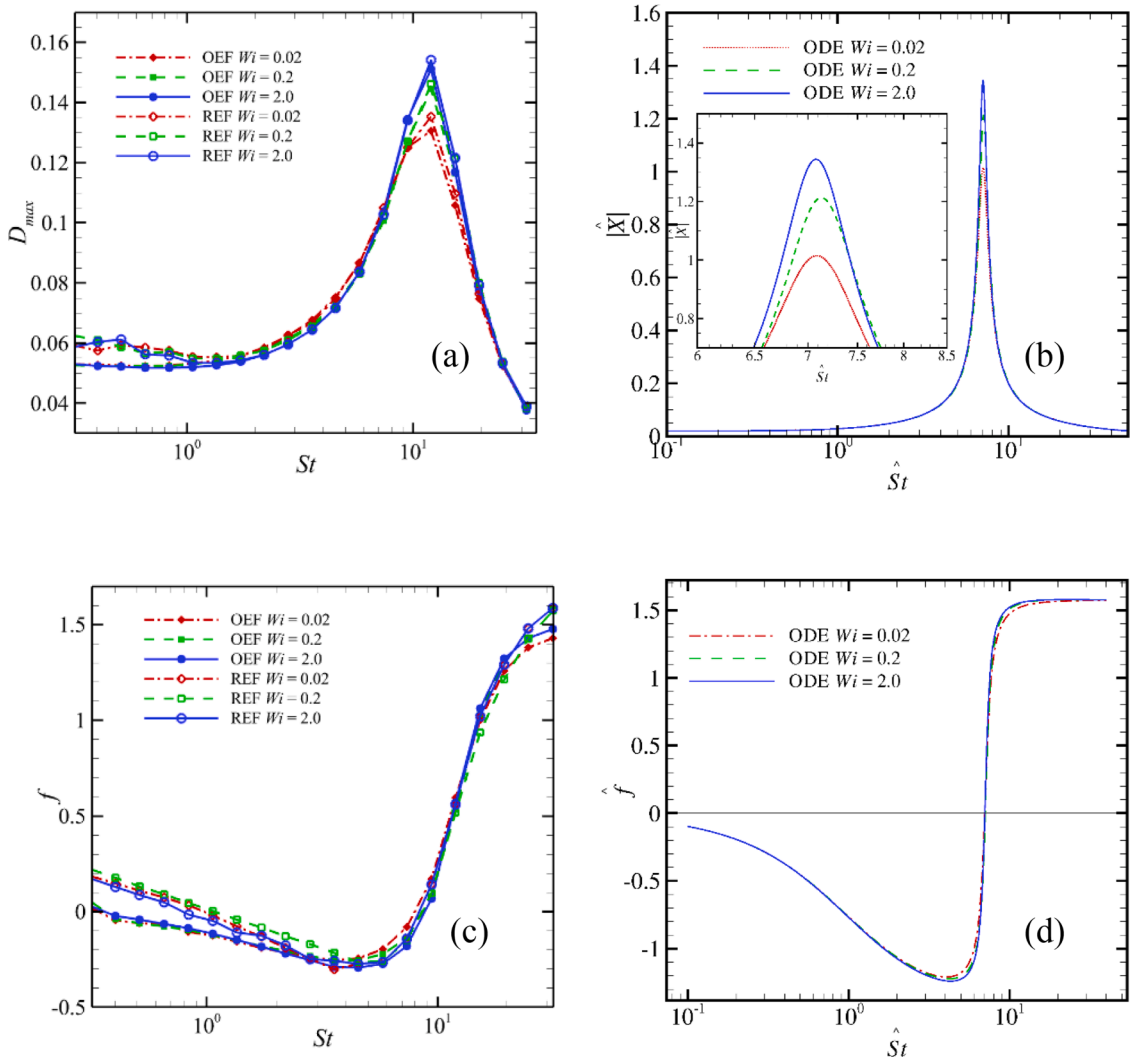

Fig. 8. Deformation vs. St for different Wi at $Re = 1.0$ and $Ca = 0.02$ in OEF and REF from DNS (a) and ODE model (b). Figure (b) inset shows detail near the peak. Phase lag vs. St for the same cases from DNS (c) and ODE model (d).

5.3. Resonance

Earlier work on Newtonian drops has shown that resonance can lead to breakups in a potential vortex at strain rates lower than those required for a steady case [31]. We see a similar tendency here for the viscoelastic case. In this section, we look at the effect of the forcing frequency (Strouhal number) on the drop deformation for different *Wi*'s. For low inertia ($Re = 0.1$) and $Ca = 0.1$, greater than the critical value for steady extension breakup (Bentley and Leal [68] experimentally found$Ca_{cr} \approx 0.13$), we obtained responses shown in Fig. 7. In contrast to

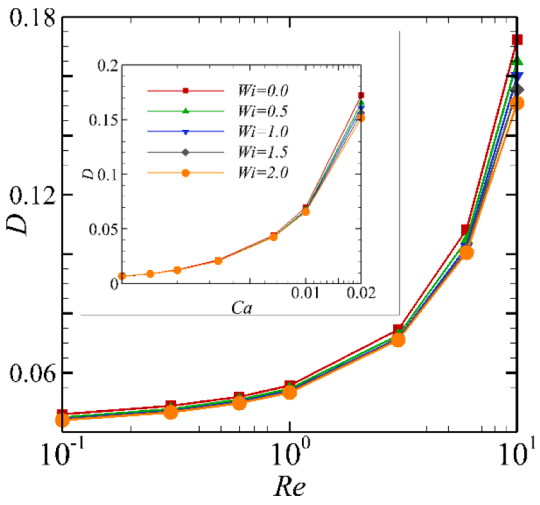

Fig. 9. Viscoelastic drop deformation at Ca = 0.2 for different Reynolds numbers in a potential vortex (St = 2). Inset shows deformation at $Re = 10$ for different Ca in a potential vortex (St = 2).

the ODE model results shown in Fig. 7(b), the numerically computed deformation doesn't show a resonance peak. It is unbounded at lower values of *St* as the drop stretches for a longer time in one period and breaks up. The ODE being a linear small deformation model cannot take this effect into account. Post-resonance for the higher *St* values, the ODE model response matches approximately with the computational results.

In Fig. 8(a) and (b), maximum deformation is plotted against *St* for different *Wi* at $Re = 1.0$ and $Ca = 0.02$, a value lower than the critical Capillary number for steady flow break up. When there is sufficient inertia we see a resonance response from the 3D simulation, which matches the prediction of the ODE model. As *Wi* is increased, we see increased deformation near the peak, but there is no change in the location of the peak in both the simulation and the model. The resonance frequency is not affected by the Weissenberg number in either case. At lower *St,* below the resonance, $D_{\max}$ decreases slightly with the increase of *Wi* whereas at higher *St*, $D_{\max}$ increases with the increase of *Wi*. Depending on the relaxation time, it takes a certain amount of time to develop the viscoelastic stresses inside the drop to inhibit drop deformation. Although at lower *St* the drop gets sufficient time to stretch, the viscoelastic stresses also can adequately develop to hinder drop deformation. At higher Strouhal numbers, a drop does not get a sufficient amount of time to develop the viscoelastic stresses and shows higher deformation with the increase of *Wi* due to an initial overshoot. The phase behavior is shown in Fig. 8(c) and (d) with a good match by the ODE model. For lower *St*, below the resonance frequency, one sees a negative phase, indicating the drop response lagging the forcing flow, whereas, above the resonance frequency, the phase is positive as is expected in such a system with inertia, approaching $\pi/2$ for large *St*(also seen in Eq. (12)). Note that such a phase advance response gives rise to unusual behaviors such as negative normal stress elasticity in oscillatory extensional rheology of a viscous emulsion [34].

Viscoelasticity with a relaxation time λ in the drop phase introduces a shear modulus of elasticity $G = \mu_d/\lambda$. In the presence of inertia, shear elasticity gives rise to the possibility of shear waves propagating inside the drop with a shear wave velocity $c_s = \sqrt{G/\rho_d}$, i.e., a wavelength of $l_w = 2\pi c_s/\omega$, or upon nondimensionalization, $l_w/a = (2\pi/St)(\lambda/\lambda_\rho)/\sqrt{\mathrm{Re}Wi}$. Similar to normal modes in an oscillating string, the wave effect is expected to be dominant for $l_w/a \sim O(1)$, when there could be internal resonances of the shear wave system affecting the drop response. These effects intrinsic to an extended medium are not accounted for in the ODE model possibly explaining the observed differences between the simulated response and that of the ODE model.

5.4. Drop breakup

With the extension axis rotating in REF, the drop doesn't experience extension at the same point on the drop interface for a long time. One can therefore expect that the drop breakup will be inhibited in a rotating extensional flow. Here we briefly consider viscoelastic effects on drop breakup in a potential vortex which is a special case of REF with $St = 2$ and is readily realizable. We plot the steady state drop deformation in Fig. 9 showing its increase with both *Re* and *Ca* (inset), as can be expected. In both cases, viscoelasticity reduces drop deformation as was also seen in steady shear [25]. However, in the presence of periodic forcing, the dynamics are governed by the subtle balance between interfacial tension, polymeric stresses, and inertia. For a particular set of *Re* and *Wi,* there exists a critical *Ca* number above which a drop breaks up. However, computationally finding Ca_{cr} poses a challenge as has been noted in our previous studies involving breakup [20,25,31] due to its sensitivity to grid resolution [31]. Here, lower bounds (upper bounds) were achieved by decreasing (increasing) *Ca* until the drop shows bounded (unbounded) deformation for five different progressively refined grid resolutions considered [31].

Fig. 10(a) and (b) show the effect of viscoelasticity on Ca_{cr} at $Re = 0.1$ and $Re = 10.0$. Below the lower bound (the curve) the drops remain bounded for all resolutions considered whereas above the upper bound,

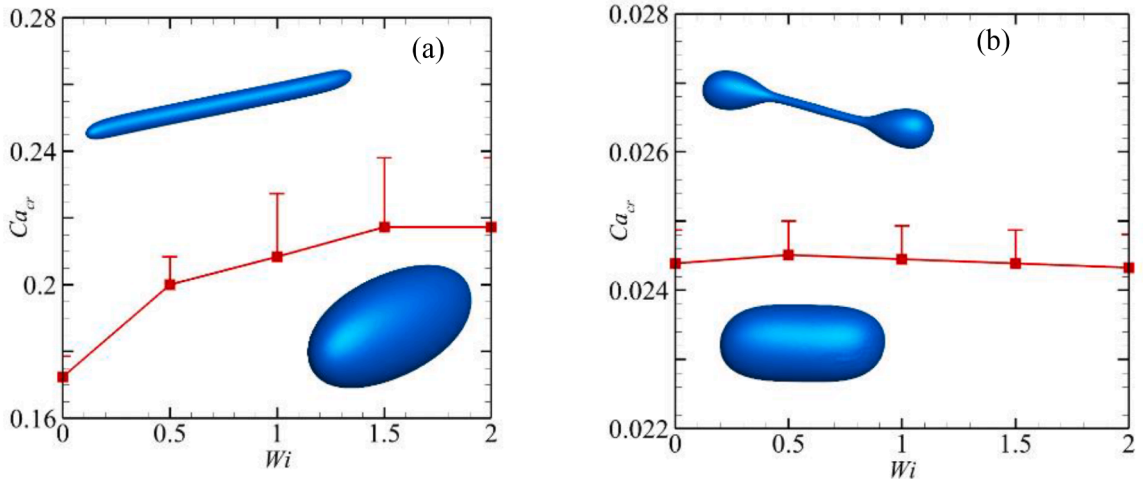

Fig. 10. (a) Shows critical capillary number at $Re = 0.1$, inset shows corresponding drop shapes above and below critical condition at Wi = 1.5, St = 2 (b) shows the critical capillary number at $Re = 10.0$, inset shows corresponding drop shapes above and below Ca critical at Wi = 1.5, St = 2.

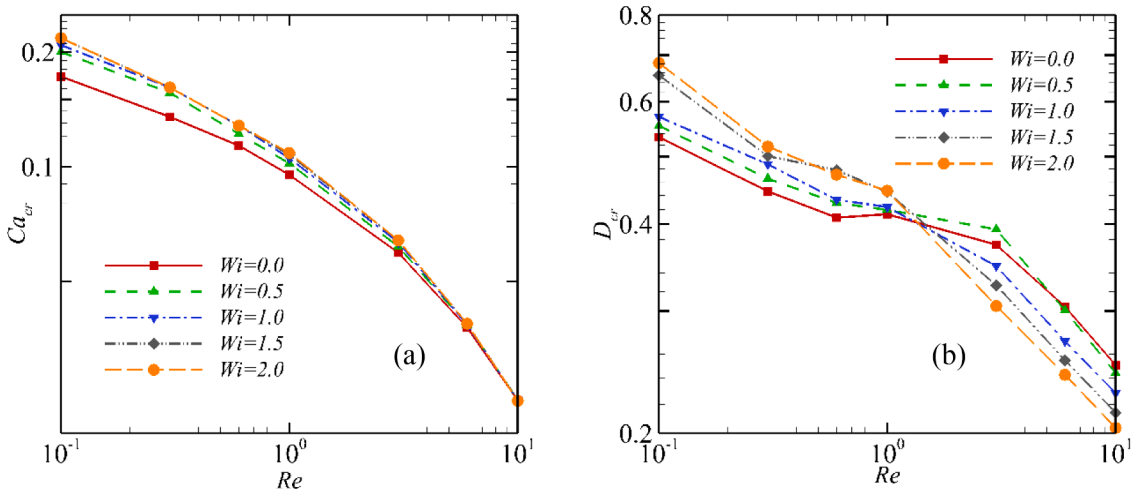

Fig. 11. (a) Shows critical Ca (lower bounds) at St = 2 and (b) shows corresponding steady-state drop deformation.

all resolutions led to unbounded deformation. At, lower inertia, Ca_{cr} increases with *Wi* indicating that viscoelasticity inhibits drop breakup. A viscoelastic drop deforms into a slender drop before breaking up at lower *Re* (Fig. 10(a) inset). In contrast, at higher inertia, Ca_{cr} doesn't change with *Wi* (at least the range of *Wi* that has been considered for this study) as drop deformation and breakup are primarily dominated by inertia (Fig. 10b). At higher inertia a viscoelastic drop forms a dumbbell shape (Fig. 10(b) inset)) before breaking up.

Fig. 11(a) and (b) show the effect of viscoelasticity on Ca_{cr} and corresponding D_{cr} at different *Re*. For all *Wi*, Ca_{cr} decreases with increasing inertia (Fig. 11a). Viscoelasticity increases Ca_{cr} hindering breakup for each *Re*, the effects diminishing with increasing *Re*. However, the critical deformation D_{cr} at that capillary number shows an increase with increasing viscoelasticity, i.e., even a more deformed drop at this higher *Ca*, does not break up due to the material elasticity aiding the interfacial tension. On the other hand, at higher *Re*, inertia dominates drop deformation and breakup indicating very little effects of *Wi* on Ca_{cr} (Fig. 11a). Correspondingly, D_{cr} decreases with the increasing *Wi* at higher inertia due to the inhibitive effect of the drop phase viscoelasticity on deformation at the same *Ca*. (also see Fig. 9).

6. Conclusion

The deformation and breakup of a viscoelastic (FENE-MCR) drop in two different time-periodic extensional flows have been numerically simulated to elucidate complex dynamics governed by the subtle competition between the periodicity, inertia, interfacial tension, and viscoelasticity. A second-order ODE model was shown to at least qualitatively capture the variation trends of drop deformation and the phase lag of its response. We also simulated drop breakup to show that viscoelasticity inhibits drop breakup by increasing the critical capillary number for breakup. At lower inertia, a drop deforms into a slender drop before breakup whereas at higher inertia it assumes a dumbbell shape.

Declaration of Competing Interest

The authors don't have any conflict of interest.

Data availability

The datasets generated and/or analyzed during the current study are available from the corresponding author upon reasonable request.

Acknowledgments

The authors acknowledge partial support from the NSF award 2019507. They acknowledge time on the Pegasus cluster at GWU. The computation was also performed using the Comet cluster at the San Diego Supercomputer Center, through the Extreme Science and Engineering Discovery Environment (XSEDE) program [69], which is supported by the National Science Foundation grant number ACI-1548562 (CTS180042).

References

[1] G.I. Taylor, The viscosity of a fluid containing small drops of another fluid, Proc. R. Soc. London. Series A, Contain. Pap. Math. Phys. Character 138 (1932) 41–48.
[2] G.I. Taylor, The formation of emulsions in definable fields of flow, Proc. R. Soc. London Series a-Math. Phys. Sci. 146 (1934) 0501–0523.
[3] R.K. Singh, K. Sarkar, Effects of viscosity ratio and three dimensional positioning on hydrodynamic interactions between two viscous drops in a shear flow at finite inertia, Phys. Fluids 21 (2009), 103303.
[4] A. Tarafder, A.R. Malipeddi, K. Sarkar, Pair interactions between viscous drops in a viscoelastic matrix in free shear: transition from passing to tumbling trajectories, J. Rheol. (N Y N Y) 66 (2022) 571–584.
[5] P. Srivastava, A.R. Malipeddi, K. Sarkar, Steady shear rheology of a viscous emulsion in the presence of finite inertia at moderate volume fractions: sign reversal of normal stress differences, J. Fluid Mech. 805 (2016) 494–522.
[6] A.R. Malipeddi, K. Sarkar, Shear-induced collective diffusivity down a concentration gradient in a viscous emulsion of drops, J. Fluid Mech. 868 (2019) 5–25.
[7] H.P. Grace, Dispersion phenomena in high-viscosity immiscible fluid systems and application of static mixers as dispersion devices in such systems, Chem. Eng. Commun. 14 (1982) 225–277.
[8] A. Acrivos, The breakup of small drops and bubbles in shear flows, Ann. N. Y. Acad. Sci. 404 (1983) 1–11.
[9] J.M. Rallison, The deformation of small viscous drops and bubbles in shear flows, Annu. Rev. Fluid Mech. 16 (1984) 45–66.
[10] H.A. Stone, Dynamics of drop deformation and breakup in viscous fluids, Annu. Rev. Fluid Mech. 26 (1994) 65–102.
[11] S. Ramaswamy, L.G. Leal, The deformation of a Newtonian drop in the uniaxial extensional flow of a viscoelastic liquid, J. Nonnewton. Fluid Mech. 88 (1999) 149–172.
[12] E.M. Toose, B.J. Geurts, J.G.M. Kuerten, A boundary integral method for 2-dimensional (Non)-Newtonian drops in slow viscous-flow, J. Nonnewton. Fluid Mech. 60 (1995) 129–154.
[13] P.T. Yue, et al., Viscoelastic effects on drop deformation in steady shear, J. Fluid Mech. 540 (2005) 427–437.
[14] P.T. Yue, et al., Transient drop deformation upon start up shear in viscoelastic fluids, Phys. Fluids 17 (2005) 12.
[15] P.T. Yue, et al., Diffuse-interface simulations of drop coalescence and retraction in viscoelastic fluids, J. Nonnewton. Fluid Mech. 129 (2005) 163–176.
[16] Schowalter, W.R., *Mechanics of Non-Newtonian Fluids* 1978, Oxford: Pergamon Press.
[17] T. Tavgac, Ph.D thesis (Chemical Engineering), Univ. of Houston, Texas, 1972.
[18] R.W. Flumerfelt, Drop breakup in simple shear fields of viscoelastic fluids, Ind. Eng. Chem. Fundamentals 11 (1972) 312–318.
[19] J.J. Elmendorp, R.J. Maalcke, A study on polymer blending microrheology. 1, Polymer Eng. Sci. 25 (1985) 1041–1047.

[20] N. Aggarwal, K. Sarkar, Effects of matrix viscoelasticity on viscous and viscoelastic drop deformation in a shear flow, J. Fluid Mech. 601 (2008) 63–84.
[21] W. Milliken, L. Leal, Deformation and breakup of viscoelastic drops in planar extensional flows, J. Nonnewton. Fluid Mech. 40 (1991) 355–379.
[22] A.S. Hsu, L.G. Leal, Deformation of a viscoelastic drop in planar extensional flows of a Newtonian fluid, J. Nonnewton. Fluid Mech. 160 (2009) 176–180.
[23] S. Ramaswamy, L.G. Leal, The deformation of a viscoelastic drop subjected to steady uniaxial extensional flow of a Newtonian fluid, J. Nonnewton. Fluid Mech. 85 (1999) 127–163.
[24] H. Li, U. Sundararaj, Does drop size affect the mechanism of viscoelastic drop breakup? Phys. fluids 20 (2008), 053101.
[25] N. Aggarwal, K. Sarkar, Deformation and breakup of a viscoelastic drop in a Newtonian matrix under steady shear, J. Fluid Mech. 584 (2007) 1–21.
[26] S. Mukherjee, K. Sarkar, Effects of viscosity ratio on deformation of a viscoelastic drop in a Newtonian matrix under steady shear, J. Nonnewton. Fluid Mech. 160 (2009) 104–112.
[27] K. Verhulst, et al., Influence of viscoelasticity on drop deformation and orientation in shear flow. Part 2: dynamics, J. Nonnewton. Fluid Mech. 156 (2009) 44–57.
[28] K. Verhulst, et al., Influence of viscoelasticity on drop deformation and orientation in shear flow part 1. Stationary states, J. Nonnewton. Fluid Mech. 156 (2009) 29–43.
[29] D. Wang, et al., A lattice Boltzmann modeling of viscoelastic drops' deformation and breakup in simple shear flows, Phys. Fluids 32 (2020), 123101.
[30] K. Sarkar, W.R. Schowalter, Deformation of a two-dimensional viscoelastic drop at non-zero Reynolds number in time-periodic extensional flows, J. Nonnewton. Fluid Mech. 95 (2000) 315–342.
[31] X. Li, K. Sarkar, Drop deformation and breakup in a vortex at finite inertia, J. Fluid Mech. 564 (2006) 1–23.
[32] R.W. Hooper, et al., Transient polymeric drop extension and retraction in uniaxial extensional flows, J. Nonnewton. Fluid Mech. 98 (2001) 141–168.
[33] X. Li, K. Sarkar, Drop dynamics in an oscillating extensional flow at finite Reynolds numbers, Phys. Fluids 17 (2005), 027103.
[34] X. Li, K. Sarkar, Negative normal stress elasticity of emulsions of viscous drops at finite inertia, Phys. Rev. Lett. 95 (2005), 256001.
[35] X. Li, K. Sarkar, Numerical investigation of the rheology of a dilute emulsion of drops in an oscillating extensional flow, J. Nonnewton. Fluid Mech. 128 (2005) 71–82.
[36] B. Bentley, L. Leal, A computer-controlled four-roll mill for investigations of particle and drop dynamics in two-dimensional linear shear flows, J. Fluid Mech. 167 (1986) 219–240.
[37] H.A. Stone, B. Bentley, L. Leal, An experimental study of transient effects in the breakup of viscous drops, J. Fluid Mech. 173 (1986) 131–158.
[38] H.A. Stone, L.G. Leal, Relaxation and breakup of an initially extended drop in an otherwise quiescent fluid, J. Fluid Mech. 198 (1989) 399–427.
[39] J. Deiber, W. Schowalter, The potential vortex as a prototype for predictions of polymer behavior in unsteady and turbulent flows. Theoretical and Applied Rheology, Elsevier, 1992, pp. 138–140.
[40] G. Brenn, S. Teichtmeister, Linear shape oscillations and polymeric time scales of viscoelastic drops, J. Fluid Mech. 733 (2013) 504–527.
[41] D.B. Khismatullin, A. Nadim, Shape oscillations of a viscoelastic drop, Phys. Rev. E 63 (2001), 061508.
[42] L. Yang, et al., Determination of dynamic surface tension and viscosity of non-Newtonian fluids from drop oscillations, Phys. Fluids 26 (2014), 113103.
[43] S.O. Unverdi, G. Tryggvason, A front-tracking method for viscous, incompressible, multi-fluid flows, J. Comput. Phys. 100 (1992) 25–37.
[44] G. Tryggvason, et al., A front-tracking method for the computations of multiphase flow, J. Comput. Phys. 169 (2001) 708–759.
[45] X.Y. Li, K. Sarkar, Effects of inertia on the rheology of a dilute emulsion of drops in shear, J. Rheol. (N Y N Y) 49 (2005) 1377–1394.
[46] X.Y. Li, K. Sarkar, Front tracking simulation of deformation and buckling instability of a liquid capsule enclosed by an elastic membrane, J. Comput. Phys. 227 (2008) 4998–5018.
[47] R.K. Singh, X.Y. Li, K. Sarkar, Lateral migration of a capsule in plane shear near a wall, J. Fluid Mech. 739 (2014) 421–443.
[48] R.K. Singh, K. Sarkar, Inertial effects on the dynamics, streamline topology and interfacial stresses due to a drop in shear, J. Fluid Mech. 683 (2011) 149–171.
[49] R.K. Singh, K. Sarkar, Hydrodynamic interactions between pairs of capsules and drops in a simple shear: effects of viscosity ratio and heterogeneous collision, Phys. Rev. E 92 (2015), 063029.
[50] N. Aggarwal, K. Sarkar, Rheology of an emulsion of viscoelastic drops in steady shear, J. Nonnewton. Fluid Mech. 150 (2008) 19–31.
[51] S. Mukherjee, K. Sarkar, Effects of viscoelasticity on the retraction of a sheared drop, J. Nonnewton. Fluid Mech. 165 (2010) 340–349.
[52] S. Mukherjee, K. Sarkar, Viscoelastic drop falling through a viscous medium, Phys. Fluids 23 (2011), 013101.
[53] S. Mukherjee, K. Sarkar, Lateral migration of a viscoelastic drop in a Newtonian fluid in a shear flow near a wall, Phys. Fluids 26 (2014), 103102.
[54] S. Mukherjee, et al., Shear-induced migration of a viscous drop in a viscoelastic liquid near a wall at high viscosity ratio: reverse migration, J. Nonnewton. Fluid Mech. 301 (2022), 104751.
[55] J.U. Brackbill, D.B. Kothe, C. Zemach, A continuum method for modeling surface tension, J. Comput. Phys. 100 (1992) 335–354.
[56] M.D. Chilcott, J.M. Rallison, Creeping flow of dilute polymer solutions past cylinders and spheres, J. Nonnewton. Fluid Mech. 29 (1988) 381.
[57] P.J. Coates, R.C. Armstrong, R.A. Brown, Calculation of steady-state viscoelastic flow through axisymmetric contractions with the EEME formulation, J. Nonnewton. Fluid Mech. 42 (1992) 141.
[58] H.M. Matos, M.A. Alves, P.J. Oliveira, New formulation for stress calculation: application to viscoelastic flow in a T-junction, Numer. Heat Transf., Part B: Fundam. 56 (2009) 351.
[59] G.N. Rocha, R.J. Poole, P.J. Oliveira, Bifurcation phenomena in viscoelastic flows through a symmetric 1:4 expansion, J. Nonnewton. Fluid Mech. 141 (2007) 1.
[60] P.J. Oliveira, A.I.I.P. Miranda, A numerical study of steady and unsteady viscoelastic flow past bounded cylinders, J. Nonnewton. Fluid Mech. 127 (2005) 51.
[61] M. Moyers-Gonzalez, I. Frigaard, The critical wall velocity for stabilization of plane Couetteâ€"Poiseuille flow of viscoelastic fluids, J. Nonnewton. Fluid Mech. 165 (2010) 441.
[62] M. Sahin, R.G. Owens, On the effects of viscoelasticity on two-dimensional vortex dynamics in the cylinder wake, J. Nonnewton. Fluid Mech. 123 (2004) 121.
[63] S. Mukherjee, K. Sarkar, Effects of matrix viscoelasticity on the lateral migration of a deformable drop in a wall-bounded shear, J. Fluid Mech. 727 (2013) 318–345.
[64] J.T. Davies, E.K. Rideal, Interfacial Phenomena, Academic Press, New York, 1963.
[65] K. Sarkar, W.R. Schowalter, Deformation of a two-dimensional drop at non-zero Reynolds number in time-periodic extensional flows: numerical simulation, J. Fluid Mech. 436 (2001) 177–206.
[66] K. Sarkar, W.R. Schowalter, Deformation of a two-dimensional viscous drop in time-periodic extensional flows: analytical treatment, J. Fluid Mech. 436 (2001) 207–230.
[67] S. Guido, M. Simeone, Binary collision of drops in simple shear flow by computer-assisted video optical microscopy, J. Fluid Mech. 357 (1998) 1–20.
[68] B.J. Bentley, L.G. Leal, An experimental investigation of drop deformation and breakup in steady, two-dimensional linear flows, J. Fluid Mech. 167 (1986) 241–283.
[69] J. Towns, et al., XSEDE: accelerating scientific discovery, Comput. Sci. Eng. 16 (2014) 62–74.